Modeling of a density oscillator

T. Kano* and S. Kinoshita
Graduate School of Frontier Biosciences, Osaka University, Suita 565-0871, Japan
(Received 16 October 2008; revised manuscript received 19 December 2008; published 27 October 2009)

A density oscillator is a well-known system, which exhibits relaxation oscillation. It alternately exhibits up and down flows through a pipe that connects two containers filled with fluids that have different densities. Although the up-flow, down-flow, and flow-reversal processes have been studied separately, the entire oscillatory dynamics has not been modeled quantitatively. In this study, we derive a model of a density oscillator by considering all the above mentioned processes. The model thus obtained describes the oscillatory behavior in a unified manner, and its viscosity and pipe-length dependence is well described. Moreover, for the demonstration of this model, we have extended it to describe the dynamical behaviors observed in coupled density oscillators. Thus, this model provides a general expression for density oscillators.

DOI: 10.1103/PhysRevE.80.046217 PACS number(s): 05.45.−a, 82.40.Bj, 05.90.+m

I. INTRODUCTION

Several systems that exhibit spontaneous regular rhythms exist in nature. Neural spiking, circadian rhythms, gene expression, the Belousov-Zhabotinsky reaction, and Josephson junction arrays are well-known examples of such systems [1–6]. These systems are called self-oscillatory systems [7,8], and they have been extensively studied in various scientific and engineering fields. A self-oscillatory system generally draws a limit cycle in phase space and exhibits a wide variety of behaviors such as bifurcation of oscillatory modes and entrainment between oscillators, the latter of which causes various types of synchronization [8,9]. In particular, when a system is characterized by more than two different time scales, the oscillation is called a relaxation oscillation, which is known to be highly nonlinear and dissipative [7,8].

A density oscillator is a typical system that exhibits relaxation oscillation [10–21]. Because of its simple and controllable aspect of experimental setup, it has been known as an excellent system to investigate the dynamics of relaxation oscillators. It consists of an inner container with a thin pipe or a small orifice at the bottom, which is held within an outer container (Fig. 1). The inner container is filled with a heavy fluid, while the outer one is filled with a light fluid. When the surfaces of both fluids are initially set at nearly the same height, the heavy fluid begins to flow downward through the pipe owing to the gradient of hydrostatic pressure. At a critical height, the flow loses stability and reverses; this causes the light fluid to flow upward through the pipe. At another critical height, the flow again loses stability and reverses; the heavy fluid begins to flow downward again. In this manner, the oscillation continues for more than several tens of cycles.

A quantitative study of a density oscillator was performed by Martin in 1970 [10]. He performed detailed experiments and also analyzed each up and down flow within the pipe according to Poiseuille's law [23]. He found that the experimental result of each up and down flow was generally in good agreement with his analytical result. However, the overall behavior of the oscillation was not explained by his theory because the flow-reversal processes between the up and down flows were not quantitatively described. Yoshikawa *et al.* proposed a phenomenological model that described the entire oscillatory behavior in a unified manner [11–13]. They combined the equations for the up and down flows derived by Martin [10] and derived a simple equation that is known as one of the most common phenomenological descriptions of oscillatory behaviors. Indeed, a wide variety of behaviors such as synchronization of oscillators, which occurs when several inner containers are held within an outer container [11–13,15–18], was well described by this model. However, it had a problem that the actual flow-reversal processes were not truly taken into account, and as a consequence, the parameters appearing in the model were given solely phenomenologically. Thus, the model could not properly describe how the experimental conditions affected the actual behavior of oscillations.

The mechanism of the flow-reversal process has been debated extensively. Martin considered that the flow reversal occurred owing to Rayleigh-Taylor instability [10], in which the perturbation at a static interface between two fluids increased when a heavy fluid was located above a light fluid [24]. However, in reality, the flow-reversal process cannot be explained in terms of Rayleigh-Taylor instability because the spatiotemporal dynamics during the flow reversal is generally complex. Steinbock *et al.*, on the other hand, analyzed the stability of the down flow within a pipe under several assumptions and derived the critical height for the instability

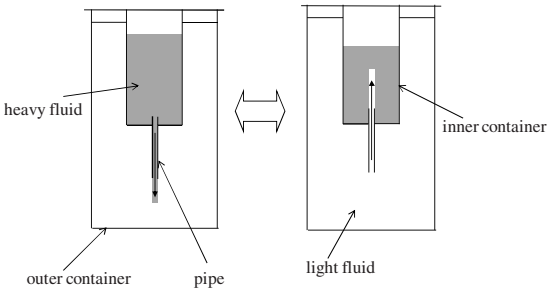

FIG. 1. Scheme of density oscillator. The down flow of the heavy fluid and the up flow of the light fluid through a pipe occur repetitively.

*takesik@fbs.osaka-u.ac.jp

 ©2009 The American Physical Society

of the flow [19]. Although their analytical results were generally in good agreement with their experimental results, the dynamics of the flow-reversal process was not described because a steady-state approximation was employed.

Recently, we have performed detailed experiments and have found that flow reversal proceeds in the following manner [21]. The flow reversal from the down to up flow, for instance, initiates from a small intrusion of light fluid at the lower end of a pipe; the intrusion grows slowly at first and then begins to increase rapidly. Finally, the tip of the intrusion reaches the upper end of the pipe and then the flow reversal is completed. Moreover, we have found that these processes are extremely sensitive to the viscosities of the fluids. Considering these experimental observations, we have proposed a model in which three essential forces acting on a unit volume element at the tip of the intrusion are considered and have found that the experimental result is well reproduced by this model. Later, we have further simplified the model so that the equations are expressed in a nondimensionalized form [22].

However, in our previous studies [21,22], the dynamics at the moment when the flow switches is not completely modeled and thus, the processes of the up and down flows have not been truly connected. For an exact description of the density oscillation, it is clearly needed to consider both up- and down-flow processes and the flow reversals between them and to properly describe how these processes are connected and how they are affected by the experimental conditions. In the present paper, we will present a unified model of a density oscillator that describes all of these processes including their viscosity and pipe-length dependence. Moreover, we will extend the model to describe the dynamical behavior of coupled density oscillators, the validity of which will be confirmed through simulations.

II. THEORETICAL MODEL FOR DENSITY OSCILLATOR

We first consider the down-flow process. We assume that the densities of the heavy and light fluids, which we denote ρ_H and ρ_L, respectively, and the viscosities of the heavy and light fluids, which we denote μ_H and μ_L, respectively, do not vary during the oscillation cycles and consider the case where the pipe length d is sufficiently larger than the pipe radius a. Moreover, we consider the case of viscous damping regime defined as $\beta\sigma^{1/2} \ll 1$, where $\beta=[ga^6\pi/(16S\mu_L^2 d)]^{1/2}$ and $\sigma=3S\delta\rho/(2a^2\pi\rho_L)$ with $\delta\rho=\rho_H-\rho_L$ and S as the surface area of the inner container [10]. A cylindrical coordinate system is employed and r and z are defined as the radial and axial coordinates, respectively. The origin of the z axis is chosen at the lower end of the pipe.

We first assume that the flow is not affected by an intrusion of the light fluid, which will be considered later. The temporal evolution of the height of the fluid surface x is derived in the same manner as was derived by Martin [10]. Although he considered the limit $R \to 0$ where R is the ratio of the surface area of the inner container to that of the outer container, here, we extend his theory to more general cases where this assumption is not necessary. When we assume that the fluid is incompressible and the flow within the pipe is parallel to the z axis, the z component of the Navier-Stokes equation is given as

$$\rho_H \frac{\partial u}{\partial t} = -\frac{\partial P(z)}{\partial z} - \rho_H g + \frac{\mu_H}{r}\frac{\partial}{\partial r}\left(r\frac{\partial u}{\partial r}\right), \tag{1}$$

where u is the z component of the velocity of the flow and $P(z)$ is the pressure. By integrating Eq. (1) over the space within the pipe, we obtain

$$\rho_H \frac{\partial \bar{u}}{\partial t} = \frac{P(0)-P(d)}{d} - \rho_H g + \left.\frac{2\mu_H}{a}\frac{\partial u}{\partial r}\right|_{r=a}, \tag{2}$$

where $\bar{u} \equiv (2/a^2)\int_0^a u(r,t) r dr$ is the average velocity within the pipe. $P(0)-P(d)$ is given as

$$P(0) - P(d) = \rho_L g h - \rho_H g(x-d) - \tfrac{3}{4}\rho_H \bar{u}|\bar{u}|, \tag{3}$$

where h is the height of the light fluid surface. The first and second terms in the right-hand side of Eq. (3) denote the difference in hydrostatic pressure, while the third term denotes the loss of pressure at the passage of a pipe, called "head loss." On the other hand, $\partial u/\partial r|_{r=a}$ is derived under the assumption of a Hagen-Poiseuille flow as described in [23] as

$$\left.\frac{\partial u}{\partial r}\right|_{r=a} = -\frac{4\bar{u}}{a}. \tag{4}$$

From the law of mass conservation, x and h are related as follows:

$$h - h_{de} = -R(x - x_{de}), \tag{5}$$

where x_{de} and h_{de} are the heights at hydrostatic equilibria when a pipe is filled with the heavy fluid, and hence, they should satisfy

$$\rho_H x_{de} = \rho_L h_{de}. \tag{6}$$

Moreover, from the condition of continuity, the following relation should hold:

$$\dot{x} = \frac{a^2\pi}{S}\bar{u}. \tag{7}$$

By substituting Eqs. (3)–(7) into Eq. (2) and considering $\dot{x} < 0$, we obtain

$$\frac{S}{a^2\pi}\ddot{x} - \frac{3S^2}{4da^4\pi^2}\dot{x}^2 + \frac{8\mu_H S}{a^4\pi\rho_H}\dot{x} + \frac{g}{d}\left(1 + \frac{\rho_L}{\rho_H}R\right)(x - x_{de}) = 0. \tag{8}$$

Note that Eq. (8) is consistent with Eq. (17) in [10] in the limit $R \to 0$. Then, since the inertia and nonlinear terms are neglected when $\beta\sigma^{1/2} \ll 1$ is satisfied (see details in [10]), the temporal evolution of x is derived from Eq. (8) as

$$\dot{x} = -\frac{(\rho_H + \rho_L R)ga^4\pi}{8\mu_H S d}(x - x_{de}). \tag{9}$$

Thus, the temporal evolution of x exhibits an exponential response if the flow is not affected by an intrusion of the light fluid.

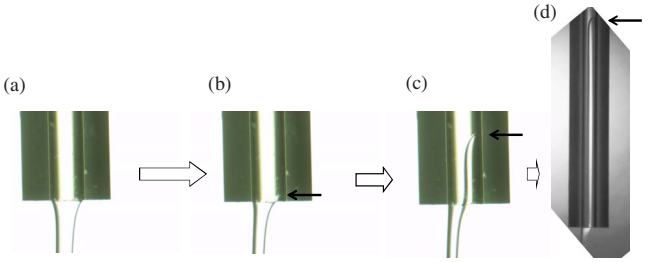

FIG. 2. (Color online) Microscopic images of the intrusion in the time course of down flow [(a)→(b)→(c)→(d)]. An intrusion of the light fluid is clearly observed (indicated by arrows). Glucose solution and water are used as the heavy and light fluids, respectively. The parameter values employed in this experiment are as follows: $a=0.365$ mm, $d=50$ mm, $R=0.337$, $\rho_H=1.064\times10^3$ kg m^{-3}, $\rho_L=0.997\times10^3$ kg m^{-3}, $\mu_H=1.42\times10^{-3}$ Pa s, and $\mu_L=0.89\times10^{-3}$ Pa s.

However, we have experimentally found in actual systems that the light fluid intrudes into a pipe before flow reversal, as shown in Fig. 2. Although the flow within the pipe is not affected by the intrusion when the intrusion length is short, the flow becomes gradually obstructed by the intrusion as it grows, which in turn causes the acceleration of the intrusion. As a consequence, the oscillatory curve of the fluid surface deviates from an exponential function (see Fig. 4). When we consider this effect, Eq. (9) will be modified as

$$\dot{x} = -[1 - q(\xi)]\frac{(\rho_H + \rho_L R)ga^4\pi}{8\mu_H Sd}(x - x_{de}), \tag{10}$$

where $q(\xi)$ is a function describing the obstruction of the flow, which causes the deviation from an exponential response. Although the functional form of $q(\xi)$ is not derived explicitly, here, we represent it phenomenologically as $q(\xi)=(\xi/d)^n$ with n being a positive constant based on the observation described above.

The temporal evolution of ξ is derived in the similar manner as that in our previous study [21]. Namely, the force acting vertically on a unit volume element located at the tip of the intrusion is divided into three forces. The first force is a viscous drag force acting downward on the interface between the two fluids; it is generated due to the velocity difference between the down flow and the growth of the intrusion. We denote this force as F_1, and it is expressed using Eqs. (7) and (10) as

$$F_1 = \frac{\mu_H + \mu_L}{2}(b_1\bar{u} - b_2\dot{\xi}) = -\frac{\mu_H + \mu_L}{2}\left[b_1[1 - q(\xi)]\frac{(\rho_H + \rho_L R)ga^2}{8d\mu_H}(x - x_{de}) + b_2\dot{\xi}\right], \tag{11}$$

where b_1 and b_2 are positive constants. It should be noted that the intrusion is resisted by the viscous drag at the interface between the two fluids, as well as by that at the pipe wall. Since we consider the latter effect in the second term on the right-hand side of Eq. (11), b_1 and b_2 are considered as independent parameters. Notice that the term including $q(\xi)$ reduces the contribution of this force, which leads to the acceleration of the intrusion [see Eq. (14)]. This is qualitatively consistent with the experimental observation.

The second force is a gravitational force and a force due to the pressure gradient, which is denoted as F_2. We have derived F_2 using Eqs. (5) and (6) as

$$F_2 = \left[\frac{\rho_L gh - \rho_H g(x-d)}{d} - \rho_L g\right](1 - e^{-\xi/\alpha}) = \left[-\frac{(\rho_H + \rho_L R)g(x - x_{de})}{d} + \delta\rho g\right](1 - e^{-\xi/\alpha}), \tag{12}$$

where the terms $\rho_L gh$ and $\rho_H g(x-d)$ are the pressures at the lower and upper ends of a pipe derived from the heights of the fluid surfaces, respectively. The term $(1-e^{-\xi/\alpha})$ is introduced to continuously connect $F_2=0$ for $\xi=0$ and $F_2=-(\rho_H+\rho_L R)g(x-x_{de})/d+\delta\rho g$ for $\xi \gg a$, with α characterizing the spatial range where F_2 takes a value between these two.

The third force is related to the effect of the acceleration of the fluid outside the pipe, which is denoted as F_3. F_3 is derived by considering the sudden contraction of the flow outside the end of the pipe that causes an intrusion of the light fluid, and hence, it is phenomenologically described by multiplying the factors $e^{-\xi/\gamma}$ and $\dot{x}^{-1}$, where γ characterizes the spatial range where this force works effectively. Thus, F_3 is derived using Eq. (10) as

$$F_3 = ke^{-\xi/\gamma}\dot{x}^{-1} \approx \frac{8kd\mu_H}{ga^2(\rho_H + \rho_L R)(x - x_{de})}e^{-\xi/\gamma}. \tag{13}$$

Here, we have neglected the term including $q(\xi)$ because this force is considered to work effectively only when $\xi \ll d$ is satisfied.

From Eqs. (11)–(13), the equation of motion for a unit volume element located at the tip of the intrusion is given as

$$\rho_L\ddot{\xi} = -\frac{\mu_H + \mu_L}{2}\left[b_1\left\{1 - \left(\frac{\xi}{d}\right)^n\right\}\frac{(\rho_H + \rho_L R)ga^2}{8d\mu_H}(x - x_{de}) + b_2\dot{\xi}\right] + \left[-\frac{(\rho_H + \rho_L R)g(x - x_{de})}{d} + \delta\rho g\right](1 - e^{-\xi/\alpha}) + \frac{8kd\mu_H}{ga^2(\rho_H + \rho_L R)(x - x_{de})}e^{-\xi/\gamma}. \tag{14}$$

Note that ξ remains zero in an exceptional case where $F_1+F_2+F_3<0$ at $\xi=0$. Thus, Eqs. (10) and (14) describe the behavior of the down flow.

The behavior of the up flow is modeled in the similar manner as the down flow. Considering the densities of the fluid flowing upward and the intrusion fluid in this case are ρ_L and ρ_H, respectively; it is straightforward to obtain the temporal evolutions of x and ξ as

$$\dot{x} = -[1 - q(\xi)]\frac{(\rho_H + \rho_L R)ga^4\pi}{8Sd\mu_L}(x - x_{ue}), \tag{15}$$

$$\rho_H\ddot{\xi} = F_1 + F_2 + F_3, \tag{16}$$

where

$$x_{ue} = x_{de} + \frac{\delta\rho d}{\rho_H + \rho_L R}, \tag{17}$$

$$q(\xi) = \left(\frac{\xi}{d}\right)^n, \tag{18}$$

$$F_1 = \frac{\mu_H + \mu_L}{2}\left[b_1[1 - q(\xi)]\frac{(\rho_H + \rho_L R)ga^2}{8d\mu_L}(x - x_{ue}) + b_2\dot{\xi}\right], \tag{19}$$

$$F_2 = \frac{(\rho_H + \rho_L R)g(x - x_{de})}{d}(1 - e^{-\xi/\alpha}), \tag{20}$$

$$F_3 = -\frac{8kd\mu_L}{ga^2(\rho_H + \rho_L R)(x - x_{ue})}e^{-\xi/\gamma}. \tag{21}$$

Here, we have considered the downward direction as positive when we define ξ, F_1, F_2, and F_3, with the origin of ξ sets at the upper end of the pipe. Note that ξ remains zero in an exceptional case where $F_1+F_2+F_3<0$ at $\xi=0$. In this manner, Eqs. (15)–(21) describe the behavior of the up flow.

Thus, the behaviors of the down and up flows are described by using two variables, x and ξ. These equations are simplified in a nondimensional form as follows. The down flow is described as

$$\phi^{-1}\frac{d\hat{x}}{d\hat{t}} = -\frac{\hat{x}}{\hat{\mu}_H}\{1 - (\epsilon\hat{\xi})^n\}, \tag{22}$$

$$\epsilon\frac{d\hat{\xi}}{d\hat{t}} = \max\left[0, -C_1\frac{\hat{x}}{\hat{\mu}_H}\{1 - (\epsilon\hat{\xi})^n\} + C_2\frac{1 - \hat{x}}{\hat{\mu}_I}(1 - e^{-\hat{\xi}/\alpha'}) + C_3\frac{\hat{\mu}_H}{\hat{\mu}_I}\frac{e^{-\hat{\xi}/\gamma'}}{\hat{x}}\right] - \frac{C_4}{\hat{\mu}_I}\frac{d^2\hat{\xi}}{d\hat{t}^2}, \tag{23}$$

while the up flow is described as

$$\phi^{-1}\frac{d\hat{x}}{d\hat{t}} = \frac{1 - \hat{x}}{\hat{\mu}_L}\{1 - (\epsilon\hat{\xi})^n\}, \tag{24}$$

$$\epsilon\frac{d\hat{\xi}}{d\hat{t}} = \max\left[0, -C_1\frac{1 - \hat{x}}{\hat{\mu}_L}\{1 - (\epsilon\hat{\xi})^n\} + C_2\frac{\hat{x}}{\hat{\mu}_I}(1 - e^{-\hat{\xi}/\alpha'}) + C_3\frac{\hat{\mu}_L}{\hat{\mu}_I}\frac{e^{-\hat{\xi}/\gamma'}}{1 - \hat{x}}\right] - \frac{C_4}{\hat{\mu}_I D}\frac{d^2\hat{\xi}}{d\hat{t}^2}, \tag{25}$$

where $\epsilon=a/d\ll 1$, $\hat{\xi}=\xi/a$, $\hat{t}=\rho_H g a^4\pi/(8S\mu_W d)t$, $\hat{\mu}_H=\mu_H/\mu_W$, $\hat{\mu}_L=\mu_L/\mu_W$, $\hat{\mu}_I=\mu_I/\mu_W=(\mu_H+\mu_L)/(2\mu_W)$, $\alpha'=\alpha/a$, $\gamma'=\gamma/a$, $D=\rho_L/\rho_H$, $\phi=1+DR$, $C_1=b_1\delta\rho S/(b_2\rho_H a^2\pi)$, $C_2=8S\delta\rho/(b_2\rho_H a^4\pi)$, $C_3=64kS\mu_W/(b_2\delta\rho g^2\rho_H a^6\pi)$, and $C_4=a^5\rho_L\rho_H\pi g/(8b_2 S\mu_W^2 d^2)$. Here, μ_W is the viscosity of water at 25.0 °C, 0.89×10^{-3} Pa s. $\hat{x}$ is defined as $\hat{x}=(x-x_{de})/(x_{ue}-x_{de})$, and hence, $\hat{x}=0$ and 1 correspond to the hydrostatic equilibria where a pipe is filled with the heavy and light fluids, respectively. max[0,…] is introduced so that the exceptions described above are included in the equations.

Here, we can neglect the last terms in the right-hand sides of Eqs. (23) and (25) under the following consideration: the ratio of C_4 to C_2 is given as

$$\frac{C_4}{C_2} = \frac{a^9\pi^2\rho_H^2\rho_L g}{64S^2\delta\rho\mu_W^2 d^2} = \frac{3}{8}(\beta\sigma^{1/2})^2\epsilon\sigma^{-2}\left(\frac{\mu_L}{\mu_W D}\right)^2. \tag{26}$$

Here, $\beta\sigma^{1/2}\ll 1$ and $\epsilon\ll 1$ are satisfied in the present assumption and $\sigma>3/2$ should be satisfied so that an oscillation occurs (see details in [10]). Moreover, $\mu_L/(\mu_W D)$ is usually not much larger than unity. Hence, $C_4/C_2\ll 1$ is satisfied, and thus, the contributions of the last terms in the right-hand sides of Eqs. (23) and (25) are considered to be negligible as compared to the term max[0,…].

Finally, we will combine the equations for the down and up flows so that the entire oscillatory behavior can be described in a unified manner. For this purpose, we have observed how the processes of the down and up flows are connected and have found that it proceeds in the following way: as the intrusion grows, the flow becomes gradually obstructed which leads to the termination of the flow. After then, the intrusion reaches the end of the pipe and the opposite flow begins. Although this opposite flow is weak at first, it becomes firm gradually, and then the flow reversal is completed. Here, the interval between the time when the flow terminates and the time when the flow reversal is completed is generally less than ~2% of the oscillation period. Thus, the switching of the down and up flows occurs in a sufficiently short time compared with the time scale of oscillation.

Based on this observation, we assume in the theory that the flow switches discontinuously when the intrusion reaches the end of the pipe. Thus, by introducing a discontinuous variable θ that takes a value of 1 or 0 during the up or down flows, respectively, Eqs. (22)–(25) are combined into the following equations:

$$\phi^{-1}\frac{d\hat{x}}{d\hat{t}} = [1 - (\epsilon\hat{\xi})^n]\frac{\theta - \hat{x}}{\hat{\mu}_H - \delta\hat{\mu}\theta}, \tag{27}$$

$$\epsilon\frac{d\hat{\xi}}{d\hat{t}} = \max\left[0, (1-2\theta)\left\{C_1\frac{[1 - (\epsilon\hat{\xi})^n](\theta - \hat{x})}{\hat{\mu}_H - \delta\hat{\mu}\theta} + C_2\frac{1 - \theta - \hat{x}}{\hat{\mu}_I}(1 - e^{-\hat{\xi}/\alpha'}) - C_3\frac{\hat{\mu}_H - \delta\hat{\mu}\theta}{\hat{\mu}_I}\frac{e^{-\hat{\xi}/\gamma'}}{\theta - \hat{x}}\right\}\right] - \epsilon^{-1}\delta(\hat{\xi} - \epsilon^{-1}), \tag{28}$$

$$\frac{d\theta}{d\hat{t}} = (1 - 2\theta)\delta(\hat{\xi} - \epsilon^{-1}), \tag{29}$$

where $\delta\hat{\mu}=\widehat{\mu_H}-\widehat{\mu_L}$. Note that θ changes its value and $\hat{\xi}$ is reset to zero when the intrusion reaches the end of the pipe,

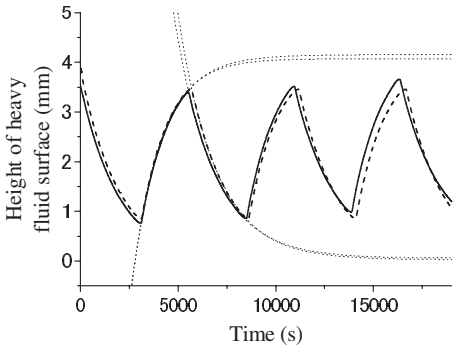

FIG. 3. Temporal evolution of the height of the heavy fluid surface. Experimental and simulated results are shown as solid and dashed lines, respectively. Each branch for the up and down flows is well fitted by an exponential function both in the experiment and the simulation (dotted line). The parameter values employed in the experiment and simulation are as follows: $a=0.365$ mm, $d=70$ mm, $R=1.44\times10^{-2}$, $\rho_H=1.059\times10^3$ kg m^{-3}, $\rho_L=0.997\times10^3$ kg m^{-3}, $\mu_H=2.64\times10^{-3}$ Pa s, $\mu_L=1.98\times10^{-3}$ Pa s, $b_1=8.03\times10^7$ m^{-2}, $b_2=1.20\times10^9$ m^{-2}, $k=0.41$ kg m^{-1} s^{-3}, $\alpha'=1.82$, $\gamma'=0.30$, $C_1=7.21$, $C_2=5.39$, and $C_3=0.32$.

that is, $\hat{\xi}=\epsilon^{-1}$. Thus, Eqs. (27)–(29) are the fundamental equations describing the overall behavior of density oscillation.

III. COMPARISON WITH THE EXPERIMENTS

We will compare the oscillatory curves simulated using the above model with those obtained in the experiments. The detailed experimental setup and procedure have already been described in [21]. In the simulation, the Runge-Kutta method is used with a time step of 0.0001. The parameters α' and γ' are chosen such that the intrusion length where its rapid growth begins is well reproduced (see Fig. 10 in [21]), while b_1, b_2, and k are chosen such that the viscosity-dependent flow-reversal process is well reproduced (see Fig. 8 in [21]). The parameter n is set at 2 to properly characterize the extent of the obstruction of flow (see Fig. 4). These parameter values do not depend on the simulation conditions described below.

First, we show the case where the viscosities of the two fluids do not differ much from each other. Figure 3 shows the experimental and simulated results for the temporal evolution of the heavy fluid surface. It is found in both the experiment and simulation that the fluid surface oscillates regularly. Each up and down flow observed in the experiment is well fitted by an exponential function, whose time constant and asymptotic value in the simulation are surprisingly in good agreement with the experiment. Moreover, the simulation also reproduces the timing of the flow reversal quite well. Thus, the overall wave form of the oscillation in the simulation is almost consistent with that in the experiment under the given parameter values. It is noted that although the average height observed in the experiment exhibits a gradual increase owing to the decrease in the density of the heavy fluid, it is not found in the simulation because the density is assumed to be kept constant.

Figure 4 shows the magnified views of Fig. 3 at the flow reversals from down to up and up to down flows, where the temporal evolution of the intrusion length is also shown. First, we observe the flow-reversal process from down to up flow in the experiment [Fig. 4(a)]. It is found that the intrusion of the light fluid begins long before the flow reversal

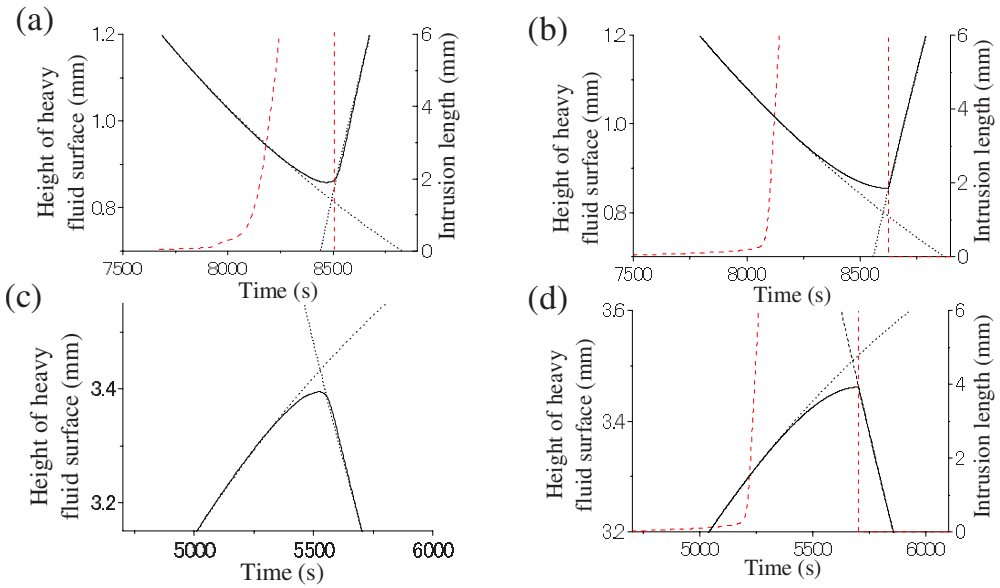

FIG. 4. (Color online) Temporal evolutions of the height of the heavy fluid surface (black solid line) and the intrusion length [red (gray) dashed line] at the flow reversal: (a) experimental and (b) simulated results for the down to up flow and (c) experimental and (d) simulated results for the up to down flow. Each branch for the up and down flows of the heavy fluid surface deviates from an exponential function (dotted line) before the flow reversal. The parameter values employed in the experiment and simulation are as follows: $a=0.365$ mm, $d=70$ mm, $R=1.44\times10^{-2}$, $\rho_H=1.059\times10^3$ kg m^{-3}, $\rho_L=0.997\times10^3$ kg m^{-3}, $\mu_H=2.64\times10^{-3}$ Pa s, $\mu_L=1.98\times10^{-3}$ Pa s, $b_1=8.03\times10^7$ m^{-2}, $b_2=1.20\times10^9$ m^{-2}, $k=0.41$ kg m^{-1} s^{-3}, $\alpha'=1.82$, $\gamma'=0.30$, $n=2$, $C_1=7.21$, $C_2=5.39$, and $C_3=0.32$.

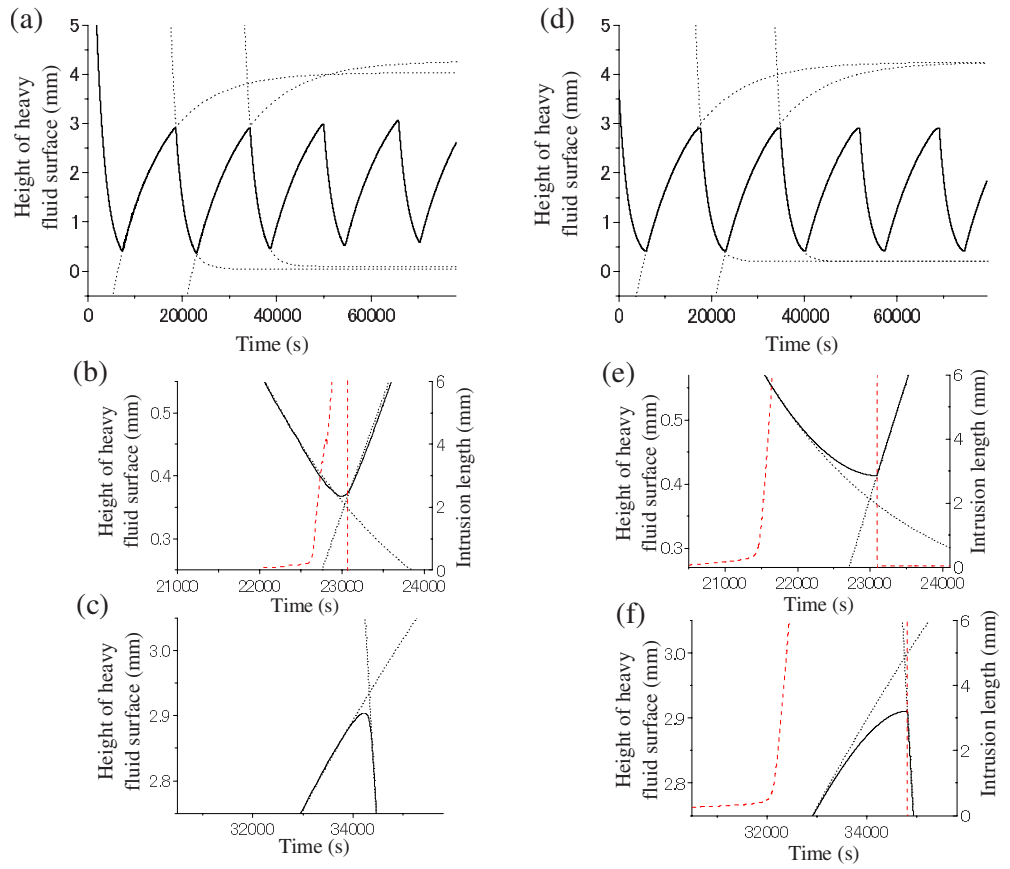

FIG. 5. (Color online) Temporal evolution of the height of the heavy fluid surface (black solid line) and the intrusion length [red (gray) dashed line] when $\mu_H \ll \mu_L$: (a)–(c) experiment and (d)–(f) simulation. (b) and (e) Magnified views at the flow reversal from down to up flow. (c) and (f) Magnified views at the flow reversal from up to down flow. Each branch for the up and down flows of the heavy fluid surface is well fitted by an exponential function (dotted line). The parameter values employed in the experiment and the simulation are as follows: $a=0.365$ mm, $d=70$ mm, $R=1.44\times10^{-2}$, $\rho_H=1.058\times10^3$ kg m^{-3}, $\rho_L=0.996\times10^3$ kg m^{-3}, $\mu_H=2.66\times10^{-3}$ Pa s, $\mu_L=14.18\times10^{-3}$ Pa s, $b_1=8.03\times10^7$ m^{-2}, $b_2=1.20\times10^9$ m^{-2}, $k=0.41$ kg m^{-1} s^{-3}, $\alpha'=1.82$, $\gamma'=0.30$, $n=2$, $C_1=7.21$, $C_2=5.39$, and $C_3=0.32$.

and grows rather slowly. When the intrusion length becomes ~1 mm, the intrusion begins to grow rapidly and accelerates gradually as the intrusion length increases. Then, the oscillatory curve of the fluid surface begins to deviate from the exponential function. Finally, when the intrusion reaches the upper end of the pipe, the flow reverses completely within ~20 s. The flow reversal from the up to down flow proceeds in a manner similar to the reversal from the down to up flow.

These tendencies are generally well reproduced by the simulation. The intrusion length ξ increases slowly at first and then begins to increase rapidly when ξ becomes ~1 mm. The deviation of the oscillatory curve of the fluid surface from the exponential function occurs during the rapid growth of the intrusion. The switching between the down and up flows occurs at $\xi=d$, which well characterizes the experimental result that the flow reverses immediately after the intrusion reaches the end of the pipe. However, the time required for the rapid growth of the intrusion is somewhat longer in the simulation than in the experiment.

Next, we show the case where the viscosities of the fluids are varied. Figures 5(a)–5(c) show the experimental result when $\mu_H \ll \mu_L$. The time constant of an exponential curve for the up flow is significantly greater than that when μ_L is small. In the flow reversal from the up to down flow, the flow reverses for a relatively low fluid surface. On the other hand, in the flow reversal from the down to up flow, the flow reversal does not occur until the fluid surface approaches the hydrostatic equilibrium. Figures 5(d)–5(f) show the simulated result. It is found that the general trend observed in the experiments is well reproduced. In the simulation, however, the time required for the rapid growth at the flow reversal from the down to up flow is longer than that in the experiment, which makes the height of the fluid surface at the flow reversal slightly closer to the hydrostatic equilibrium.

Figures 6(a)–6(c) show the experimental result when $\mu_H \gg \mu_L$. A trend opposite to that when $\mu_H \ll \mu_L$ is found to occur. The time constant of the exponential curve for the down flow is significantly greater than that when μ_H is small, and the flow reversal from the down to up flow occurs when the fluid surface is still higher while that from the up to down flow does not occur until the fluid surface approaches the hydrostatic equilibrium. Figures 6(d)–6(f) show the simulated result. Although the simulated flow reversal from the up to down flow occurs when the fluid surface is slightly

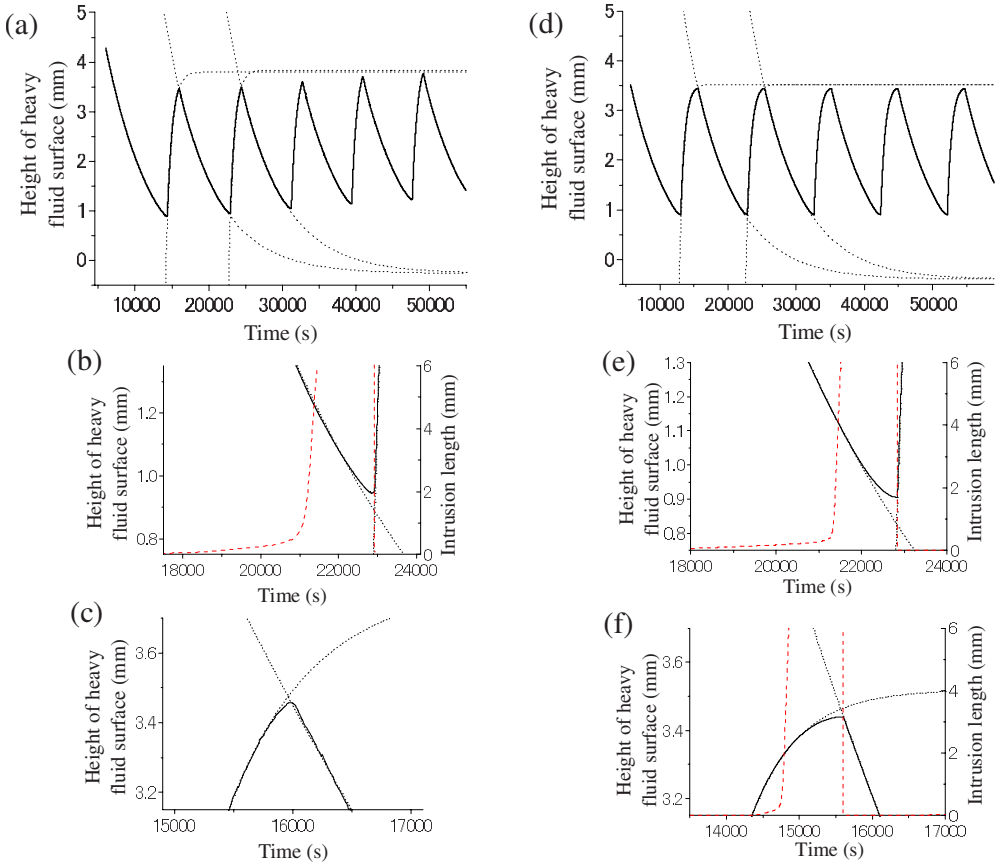

FIG. 6. (Color online) Temporal evolution of the height of the heavy fluid surface (black solid line) and the intrusion length [red (gray) dashed line] when $\mu_H \gg \mu_L$: (a)–(c) experiment and (d)–(f) simulation. (b) and (e) Magnified views at the flow reversal from down to up flow. (c) and (f) Magnified views at the flow reversal from up to down flow. Each branch for the up and down flows of the heavy fluid surface is well fitted by an exponential function (dotted line). The parameter values employed in the experiment and the simulation are as follows: $a=0.365$ mm, $d=70$ mm, $R=1.44\times10^{-2}$, $\rho_H=1.057\times10^3$ kg m^{-3}, $\rho_L=0.997\times10^3$ kg m^{-3}, $\mu_H=8.59\times10^{-3}$ Pa s, $\mu_L=0.89\times10^{-3}$ Pa s, $b_1=8.03\times10^7$ m^{-2}, $b_2=1.20\times10^9$ m^{-2}, $k=0.38$ kg m^{-1} s^{-3}, $\alpha'=1.82$, $\gamma'=0.30$, $n=2$, $C_1=6.99$, $C_2=5.23$, and $C_3=0.31$.

closer to the hydrostatic equilibrium, the general trend found in the experiment is well reproduced.

The case where the pipe length is shortened is also investigated to elucidate the applicability of the present model. Figures 7(a)–7(c) show the experimental result when a short pipe ($d=10$ mm) is used. Obviously, the wave form of the oscillation in the fluid surface is still characterized by exponential functions. The amplitude of the oscillation and the time constants of the exponential functions for each up and down flow are found to be much smaller than that in the case of a long pipe. On the other hand, the intrusion grows slowly at first and begins to grow rapidly at an intrusion length of ~1 mm, which leads to the deviation from the exponential response in the fluid surface. This is essentially the same as that for a long pipe. Figures 7(d)–7(f) show the simulated result. We find that the general trend found in the experiment is well reproduced. However, the time required for the rapid growth of an intrusion in the flow reversal is somewhat lesser than that in the experiment. In addition, the time constants of the exponential functions for both up and down flows are relatively greater than those in the experiment, which is thought to be due to the slight deviation from an ideal Hagen-Poiseuille flow [23].

IV. INTERPRETATIONS OF THEORETICAL MODEL

Thus, it is found that the overall behavior of a density oscillator is excellently expressed by the above model. From the model, the mechanism of the density oscillation is physically understandable through the following considerations. First, we consider a case of the down flow ($\theta=0$). Let $f_1(\hat{\xi})$, $f_2(\hat{\xi})$, and $f_3(\hat{\xi})$ be defined as $f_1(\hat{\xi})=-C_1\hat{x}\{1-(\epsilon\hat{\xi})^n\}/\hat{\mu}_H$, $f_2(\hat{\xi})=C_2(1-\hat{x})(1-e^{-\hat{\xi}/\alpha'})/\hat{\mu}_1$, and $f_3(\hat{\xi})=C_3\hat{\mu}_H e^{-\hat{\xi}/\gamma'}/(\hat{\mu}_1\hat{x})$, and we use $f(\hat{\xi})\equiv f_1(\hat{\xi})+f_2(\hat{\xi})+f_3(\hat{\xi})$. Note that $f_1(\hat{\xi})$, $f_2(\hat{\xi})$, and $f_3(\hat{\xi})$ originate from the forces F_1, F_2, and F_3, respectively, and that $\hat{x}$ should be regarded as a parameter characterizing their functional forms because it is a slowly varying variable as compared to $\hat{\xi}$ with respect to time. Then, Eq. (28) is simply rewritten as

$$\epsilon\frac{d\hat{\xi}}{d\hat{t}}=\max[0,f(\hat{\xi})]-\epsilon^{-1}\delta(\hat{\xi}-\epsilon^{-1}). \tag{30}$$

Figure 8 shows the $\hat{x}$ dependence of $f_1(\hat{\xi})$, $f_2(\hat{\xi})$, $f_3(\hat{\xi})$, and $f(\hat{\xi})$ when $\hat{\mu}_H=\hat{\mu}_L$, $\hat{\mu}_H>\hat{\mu}_L$, and $\hat{\mu}_H<\hat{\mu}_L$. Now, consider the case when $\hat{\mu}_H=\hat{\mu}_L$ [Figs. 8(a)–8(c)]. When the value of $\hat{x}$ is

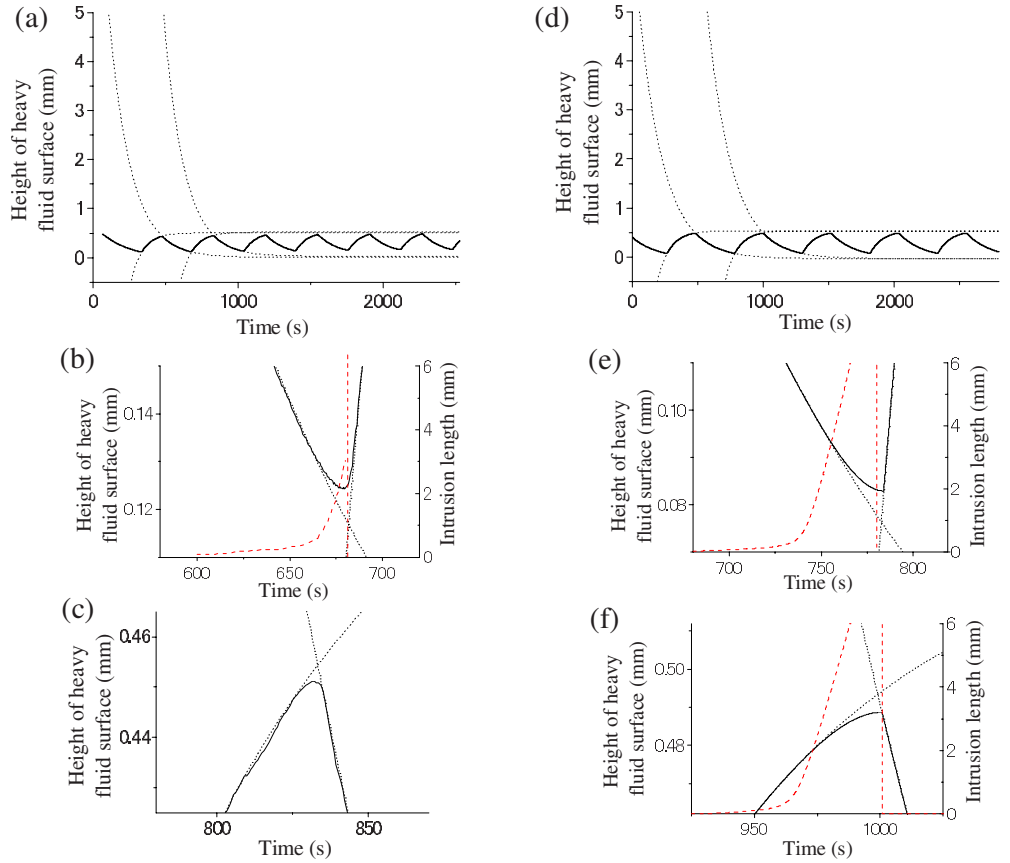

FIG. 7. (Color online) Temporal evolution of the height of the heavy fluid surface (black solid line) and the intrusion length [red (gray) dashed line] in the case of a short pipe: (a)–(c) experiment and (d)–(f) simulation. (b) and (e) Magnified views at the flow reversal from down to up flow. (c) and (f) Magnified views at the flow reversal from up to down flow. Each branch for the up and down flows of the heavy fluid surface is well fitted by an exponential function (dotted line). The parameter values employed in the experiment and the simulation are as follows: $a=0.365$ mm, $d=10$ mm, $R=1.44\times10^{-2}$, $\rho_H=1.057\times10^3$ kg m^{-3}, $\rho_L=0.996\times10^3$ kg m^{-3}, $\mu_H=1.79\times10^{-3}$ Pa s, and $\mu_L=0.89\times10^{-3}$ Pa s, $b_1=8.03\times10^7$ m^{-2}, $b_2=1.20\times10^9$ m^{-2}, $k=0.40$ kg m^{-1} s^{-3}, $\alpha'=1.82$, $\gamma'=0.30$, $n=2$, $C_1=7.10$, $C_2=5.31$, and $C_3=0.32$.

large, the intrusion does not occur and $\hat{\xi}$ remains zero because the relation $f(0)\leq 0$ should hold owing to the large contribution of $f_1(\hat{\xi})$ [Fig. 8(a)]. However, as the value of $\hat{x}$ is decreased, $f(0)$ becomes positive because the contribution of $f_3(\hat{\xi})$ becomes large and also because the contribution of $f_1(\hat{\xi})$ decreases while that of $f_2(\hat{\xi})$ increases. Then, the relation $f(\hat{\xi})=0$ leads to a positive solution $\hat{\xi}_0$ with $f'(\hat{\xi}_0)<0$. Hence, the condition $\hat{\xi}=\hat{\xi}_0$ gives a stable solution of Eq. (30) [Fig. 8(b)]. Thus, the light fluid begins to intrude into a pipe. As $\hat{x}$ is further decreased, $\hat{\xi}_0$ increases gradually. When the contribution of the sum of $f_2(\hat{\xi})$ and $f_3(\hat{\xi})$ becomes greater than that of $f_1(\hat{\xi})$, the solution $\hat{\xi}_0$ disappears so that $f(\hat{\xi})$ becomes positive for $0\leq\hat{\xi}<\epsilon^{-1}$ [Fig. 8(c)]. Thus, the intrusion accelerates suddenly. Finally, $\hat{\xi}$ is reset to zero when $\hat{\xi}$ becomes ϵ^{-1}, and then the flow reverses completely.

As one may find from the above argument, the properties that $f_2(\hat{\xi})$ and $f_3(\hat{\xi})$ are the increasing and decreasing functions of $\hat{\xi}$, respectively, are the essential points of the present model because the slow growth of the intrusion cannot be explained without them. By considering the derivation of F_2 and F_3, we find that the increasing property of $f_2(\hat{\xi})$ is originated from the fact that the pressure gradient is continuously connected between inside and outside the pipe, while the decreasing property of $f_3(\hat{\xi})$ comes from the fact that the effect of the acceleration of the fluid outside the pipe works only in the vicinity of the end of the pipe.

When the viscosities of the fluids are varied, the functional forms of $f_1(\hat{\xi})$, $f_2(\hat{\xi})$, and $f_3(\hat{\xi})$ change significantly. When $\hat{\mu}_H>\hat{\mu}_L$ [Figs. 8(d)–8(f)], $f(\hat{\xi})$ becomes relatively large especially for small $\hat{\xi}$, which is due to the relatively large contribution of $f_3(\hat{\xi})$. Thus, the intrusion and hence the onset of its rapid growth occur even when $\hat{x}$ is still large. On the other hand, when $\hat{\mu}_H<\hat{\mu}_L$ [Figs. 8(g) and 8(h)], $f(\hat{\xi})$ becomes generally small because of the relatively large contribution of $f_1(\hat{\xi})$. Hence, the intrusion and the onset of its rapid growth do not occur until $\hat{x}$ becomes sufficiently small. Such viscosity dependence is physically originated from the facts that the viscosity of the fluid at the interface $\hat{\mu}_I$ depends both on the viscosities of the heavy and light fluids while the velocity of down (up) flow depends solely on the viscosity of the heavy (light) fluid and that the effect of the acceleration

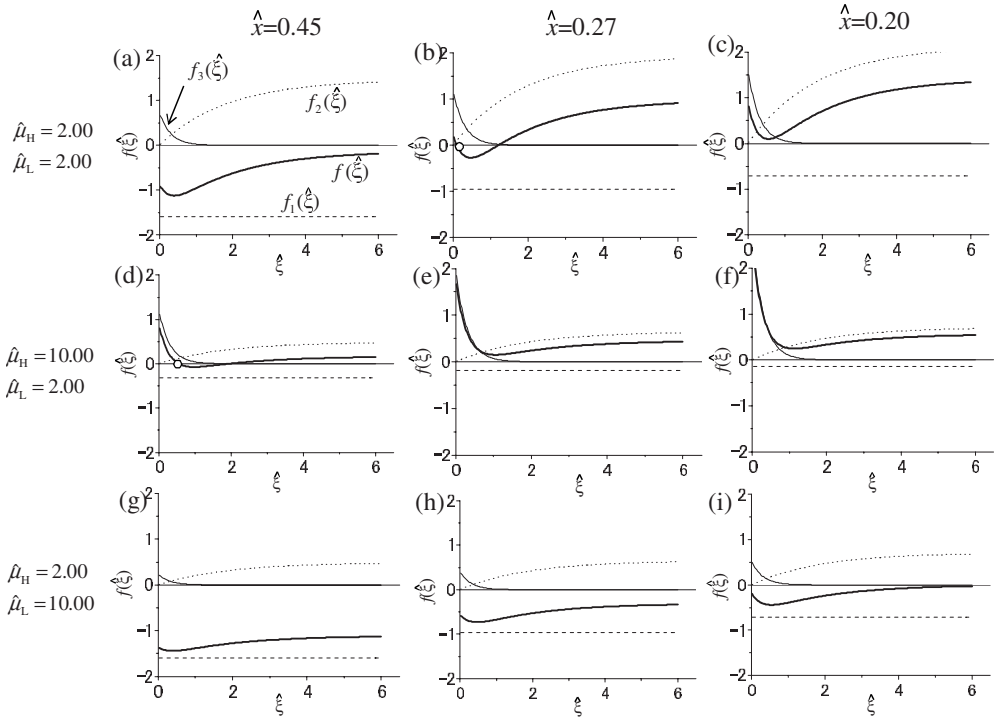

FIG. 8. Functional forms of $f_1(\hat{\xi})$ (dashed line), $f_2(\hat{\xi})$ (dotted line), $f_3(\hat{\xi})$ (solid line), and $f(\hat{\xi})$ (bold line) in the cases of (a)–(c) $\hat{\mu}_H = 2.00$ and $\hat{\mu}_L = 2.00$, (d)–(f) $\hat{\mu}_H = 10.00$ and $\hat{\mu}_L = 2.00$, and (g)–(i) $\hat{\mu}_H = 2.00$ and $\hat{\mu}_L = 10.00$. $\hat{x}$ is set as (a), (d), and (g) $\hat{x} = 0.45$, (b), (e), and (h) $\hat{x} = 0.27$, and (c), (f), and (i) $\hat{x} = 0.20$. The stable solution of Eq. (30), $\hat{\xi} = \hat{\xi}_0$, is indicated by an empty circle. The values of the parameters in the simulation are as follows: $a = 0.365$ mm, $d = 70$ mm, $\rho_H = 1.057 \times 10^3$ kg m^{-3}, $\rho_L = 0.996 \times 10^3$ kg m^{-3}, $R = 1.44 \times 10^{-2}$, $b_1 = 8.03 \times 10^7$ m^{-2}, $b_2 = 1.20 \times 10^9$ m^{-2}, $k = 0.40$ kg m^{-1} s^{-3}, $\epsilon = 5.21 \times 10^{-3}$, $\alpha' = 1.82$, $\gamma' = 0.30$, $n = 2$, $C_1 = 7.10$, $C_2 = 5.31$, and $C_3 = 0.32$.

of the flow that has passed through the pipe (F_3) is related to the velocity of the flow.

Next, let us consider the case of an up flow ($\theta = 1$). Even in this case, Eq. (28) is still described by Eq. (30) if we replace $\hat{x}$ and μ_H in $f_1(\hat{\xi})$, $f_2(\hat{\xi})$, and $f_3(\hat{\xi})$ with $1 - \hat{x}$ and μ_L, respectively. Hence, the process of the flow reversal from the up to down flow can also be explained from Fig. 8 in a manner similar to that of the flow reversal from the down to up flow.

The pipe length is only related to the parameter ϵ. Thus, the relative contributions of $f_1(\hat{\xi})$, $f_2(\hat{\xi})$, and $f_3(\hat{\xi})$ are not affected by the pipe length. Moreover, the nondimensionalized time required for the rapid growth of the intrusion is not affected by the pipe length in the model because $d\hat{\xi}/d\hat{t}$ is proportional to ϵ^{-1} during the rapid growth whereas the flow reverses at $\hat{\xi} = \epsilon^{-1}$. Thus, we find from the model that the pipe length does not essentially affect the flow-reversal process.

V. EXTENSION TO COUPLED OSCILLATORS

The model derived in Sec. II can be easily extended to describe the behavior of coupled density oscillators in which several inner containers are held within one outer container. It is well known in such systems that the dynamical behaviors of the fluid surfaces in the inner containers are affected by each other through the height of the light fluid surface h, which leads to various types of synchronization [11–13,15,17,18]. For instance, antiphase synchronization of two inner containers will occur because the down flow in one of the inner containers elevates the light fluid surface and increases the hydropressure in the outer container, which makes the flow in the other container upward and vice versa.

Now we consider a case where N inner containers are held within one outer container. We assume that the densities of the heavy fluids, the diameters of the pipes, and the surface areas of the fluid surfaces in the inner containers are all identical. Then, h is described as

$$h - h_{de} = -\sum_{j=1}^{N} R(x_j - x_{de}), \quad j = 1,2,\ldots,N, \tag{31}$$

where x_j is the height of the heavy fluid surface of the jth inner container and R is here defined as the ratio of the surface area of one of the inner containers to that of the outer container. By using Eq. (31) instead of Eq. (5), it is straightforward to derive the model of coupled oscillators as follows:

$$\frac{d\tilde{x}_i}{d\hat{t}} = [1 - \hat{q}(\xi)] \frac{\theta_i \hat{d}_i - \tilde{x}_i - DR\sum_{j=1}^{N} \tilde{x}_j}{(\hat{\mu}_{Hi} - \delta\hat{\mu}_i)\theta_i \hat{d}_i}, \tag{32}$$

$$\frac{\epsilon}{\hat{d}_i}\frac{d\hat{\xi}_i}{d\hat{t}} = \max\left[0,(1-2\theta_i)\left\{C_1\frac{[1-\hat{q}(\xi)](\theta_i\hat{d}_i-\tilde{x}_i-DR\sum_{j=1}^{N}\tilde{x}_j)}{(\hat{\mu}_{\mathrm{H}i}-\delta\hat{\mu}_i\theta_i)\hat{d}_i}+C_2\frac{(1-\theta_i)\hat{d}_i-\tilde{x}_i-DR\sum_{j=1}^{N}\tilde{x}_j}{\hat{\mu}_{\mathrm{I}i}\hat{d}_i}(1-e^{-\hat{\xi}_i/\alpha'})\right.\right.$$
$$\left.\left.-C_3\frac{\hat{\mu}_{\mathrm{H}i}-\delta\hat{\mu}_i\theta_i}{\hat{\mu}_{\mathrm{I}i}}\frac{\hat{d}_i e^{-\hat{\xi}_i/\gamma'}}{\theta\hat{d}_i-\tilde{x}_i-DR\sum_{j=1}^{N}\tilde{x}_j}\right\}\right]-\frac{\hat{d}_i}{\epsilon}\delta\left(\hat{\xi}_i-\frac{\hat{d}_i}{\epsilon}\right), \tag{33}$$

$$\frac{d\theta_i}{d\hat{t}} = (1-2\theta_i)\delta\left(\hat{\xi}_i-\frac{\hat{d}_i}{\epsilon}\right), \tag{34}$$

$$\hat{q}(\xi_i) = \left(\frac{\epsilon\hat{\xi}_i}{\hat{d}_i}\right)^n, \tag{35}$$

where $\hat{\xi}_i$ and θ_i are the nondimensionalized intrusion length and the parameter expressing the direction of flow of the ith oscillator, respectively. $\hat{\mu}_{\mathrm{H}i}$ is the nondimensionalized viscosity of the heavy fluid in the ith container and $\hat{\mu}_{\mathrm{I}i}=(\hat{\mu}_{\mathrm{H}i}+\hat{\mu}_{\mathrm{L}})/2$. $\hat{d}_i \equiv d_i/d_0$ is the nondimensionalized pipe length, where d_0 is the characteristic length of a pipe. The nondimensionalized height of the heavy fluid surface $\tilde{x}_i$ is defined as $\tilde{x}_i=(x_i-x_{\mathrm{de}})\rho_{\mathrm{H}}/\delta\rho d_0$ and ϵ is defined as $\epsilon=a/d_0$.

The results obtained from the simulations of Eqs. (32)–(34) are shown in Figs. 9–11. The time step employed here is set at 0.001. Figures 9(a) and 9(b) show the cases of $N=2$ and 3, where the properties of the pipes and the fluids in the inner containers are assumed to be identical. It is clear that the dynamics of the fluid surfaces in the inner containers are synchronized in antiphase [the phase differences of $\sim\pi$ and $\sim(2/3)\pi$, respectively]. The similar results are frequently reported so far in the experiments [11,12,15,17,18].

Figure 10 shows the case of $N=2$, where the pipe lengths and the viscosities of the fluids in the inner containers are not identical. We find in Fig. 10(a) that synchronization by the ratio in the period of 1:3 occurs. On the other hand, when $\hat{\mu}_{\mathrm{H}2}$ is slightly varied, the 1:3 synchronization disappears and the phase relationship between the two oscillators becomes rather complex [Fig. 10(b)]. Figure 11 shows the period ratio of the two inner containers when $\hat{\mu}_{\mathrm{H}2}$ is varied with R set at 0.1 and 0.3. It is clear that the period ratio increases as $\hat{\mu}_{\mathrm{H}2}$ increases, and it tends to be entrained into the simple ratio of integers such as 3:2, 1:1, 2:3, 1:2, 2:5, and 1:3. For large R, the region where the entrainment occurs becomes large and the plots of the period ratio become rather stepwise [Fig. 11(b)]. Such stepwise character is similar to a phenomenon called "devil's staircases" [8]. These results do not contradict with the previously reported experimental findings that the period ratio is entrained into the ratio of the nearest natural numbers [13] and that the ratio of the areas of the heavy and light fluid surfaces characterizes the coupling strength [15].

Thus, Eqs. (32)–(34) well describe the dynamical behavior of coupled density oscillators. In contrast to the model reported previously [11–13], the present model adequately reflects the dependence of experimental conditions such as the properties of the fluids and the geometries of the contain-

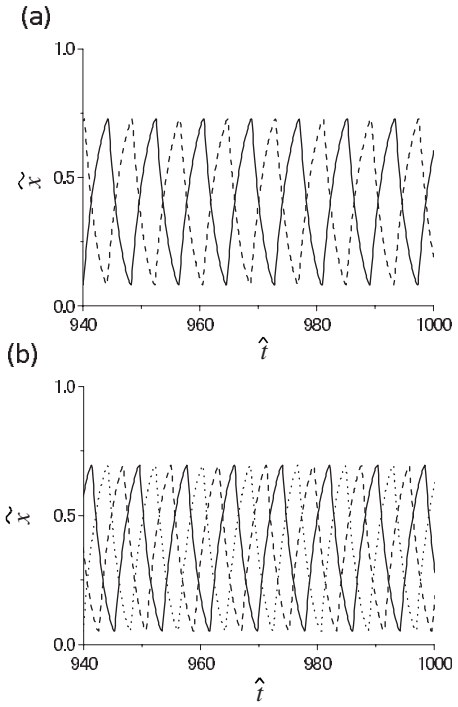

FIG. 9. Simulated results of (a) two and (b) three coupled oscillators when the pipe lengths and the viscosities of the heavy fluids are identical. The temporal evolution of $\tilde{x}_i$ for each oscillator is shown. The first, second, and third oscillators are indicated by solid, dashed, and dotted lines, respectively. The initial condition is set at $\tilde{x}_1=1$, $\tilde{x}_2=0.8$, $\tilde{x}_3=0.6$, $\hat{\xi}_1=\hat{\xi}_2=\hat{\xi}_3=0$, and $\theta_1=\theta_2=\theta_3=0$. The parameters employed in the simulation are as follows: $a=0.365$ mm, $d_0=70$ mm, $d_1=d_2=d_3=70$ mm, $\rho_{\mathrm{H}}=1.057\times10^3$ kg m^{-3}, $\rho_{\mathrm{L}}=0.996\times10^3$ kg m^{-3}, $\mu_{\mathrm{H}1}=\mu_{\mathrm{H}2}=\mu_{\mathrm{H}3}=2.00\times10^{-3}$ Pa s, $\mu_{\mathrm{L}}=2.50\times10^{-3}$ Pa s, $R=0.1$, $b_1=8.03\times10^7$ m^{-2}, $b_2=1.20\times10^9$ m^{-2}, $k=0.40$ kg m^{-1} s^{-3}, $\epsilon=5.21\times10^{-3}$, $\alpha'=1.82$, $\gamma'=0.30$, $n=2$, $C_1=7.10$, $C_2=5.31$, and $C_3=0.32$.

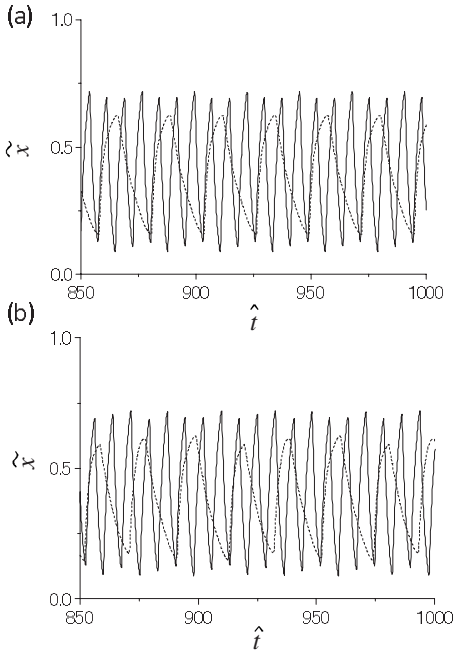

FIG. 10. Simulated results of two coupled oscillators when the pipe lengths and the viscosities of the heavy fluids are not identical. The temporal evolution of $\tilde{x}_i$ for each oscillator is shown. The first and second oscillators are indicated by solid and dashed lines, respectively. The initial condition is set at $\tilde{x}_1=1$, $\tilde{x}_2=0.8$, $\hat{\xi}_1=\hat{\xi}_2=0$, and $\theta_1=\theta_2=0$. μ_{H2} is set at (a) 15.00×10^{-3} Pa s and (b) 14.00×10^{-3} Pa s. Other parameters employed in the simulation are as follows: $a=0.365$ mm, $d_0=70$ mm, $d_1=70$ mm, $d_2=50$ mm, $\rho_H=1.057\times10^3$ kg m^{-3}, $\rho_L=0.996\times10^3$ kg m^{-3}, $\mu_{H1}=2.00\times10^{-3}$ Pa s, $\mu_L=2.50\times10^{-3}$ Pa s, $R=0.1$, $b_1=8.03\times10^7$ m^{-2}, $b_2=1.20\times10^9$ m^{-2}, $k=0.40$ kg m^{-1} s^{-3}, $\epsilon=5.21\times10^{-3}$, $\alpha'=1.82$, $\gamma'=0.30$, $n=2$, $C_1=7.10$, $C_2=5.31$, and $C_3=0.32$.

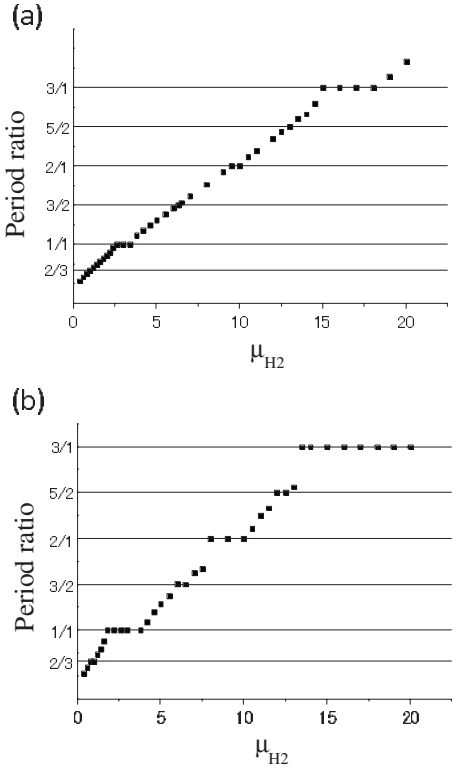

FIG. 11. Simulated result for period ratio in two coupled oscillators. The ratio of the period of the second to first oscillators is plotted against $\hat{\mu}_{H2}$, where $\hat{\mu}_{H1}$ is kept constant. (a) $R=0.1$ and (b) $R=0.3$. Solid lines indicate the period ratios of 2/3, 1/1, 3/2, 2/1, 5/2, and 3/1 from bottom to top. The parameters employed in the simulation are as follows: $a=0.365$ mm, $d_0=70$ mm, $d_1=70$ mm, $d_2=50$ mm, $\rho_H=1.057\times10^3$ kg m^{-3}, $\rho_L=0.996\times10^3$ kg m^{-3}, $\mu_{H1}=2.00\times10^{-3}$ Pa s, $\mu_L=2.50\times10^{-3}$ Pa s, $b_1=8.03\times10^7$ m^{-2}, $b_2=1.20\times10^9$ m^{-2}, $k=0.40$ kg m^{-1} s^{-3}, $\epsilon=5.21\times10^{-3}$, $\alpha'=1.82$, $\gamma'=0.30$, $n=2$, $C_1=7.10$, $C_2=5.31$, and $C_3=0.32$.

ers and pipes. Hence, it will lead us to properly understand the dynamics of coupled density oscillators in more general cases.

VI. DISCUSSION

We have derived a model of a density oscillator that describes the entire oscillatory dynamics in a unified manner. Although a phenomenological model had been reported previously [11–13], it did not contain explicit experimental parameters and it could not be used to characterize the actual behavior of oscillations because the flow-reversal process was not taken into account. On the contrary, in the present model, all the processes including the up and down flows and the flow-reversal process are treated in a unified way, and their viscosity dependence as well as the pipe-length dependence is generally well reproduced. Thus, the present model will become a general description of density oscillators.

The flow-reversal process is particularly important in a density oscillator, and it is well characterized by three forces acting on the volume element at the tip of the intrusion, F_1, F_2, and F_3. Actually, the slow growth of an intrusion followed by its rapid growth is well reproduced by considering these three forces. These forces are actually characterized by several parameters, among which α' and γ' are particularly important, because they characterize the length scales where $f_2(\hat{\xi})$ increases and $f_3(\hat{\xi})$ decreases, respectively, and hence they altogether determine the intrusion length when its rapid growth begins. These two parameters seem to have universal characteristics. In fact, our experimental observation that the onset of the rapid growth occurs at $\xi\sim1$ mm even when the viscosities and pipe length are varied is well reproduced by taking α' and γ' as constant. Moreover, the fact that the values of α' and γ' are both O(1) is physically plausible because α and γ should be the order of the pipe radius, which is expected from their physical meanings.

The function $q(\xi)$ and the discontinuous variable θ, which are introduced in the present study, are also essential for describing the connection between the up and down flows. Our experimental findings that the fluid surface gradually deviates from the exponential function as the intrusion grows and that the flow reversal is completed almost instantaneously after the intrusion reaches the end of the pipe are well reproduced by introducing $q(\xi)$ and θ, respectively.

We have also extended the model to describe the behaviors of coupled density oscillators and have shown that the behaviors observed in the previous experiments, such as an-

tiphase synchronization and synchronization by the ratio of integers [11–13,15,17,18], are actually reproduced by the simulations of the model. In contrast to the model reported previously [11–13], this model describes how the behavior changes depending on the viscosities and the pipe lengths. Moreover, it also describes the dependence of the ratio of the surface areas of the heavy fluid to that of the light fluids, which characterizes the coupling strength. Although we have considered here the case where the surface areas are identical among the inner containers, this model will be easily extended to the case where they are not identical, that is, the coupling is asymmetric.

We have noticed, however, that the present model does not reproduce the growth rate of the intrusion during the rapid growth. In fact, the time required for the rapid growth at the flow reversal from the down to up flow in the simulation is generally longer than that in the experiment [see Figs. 4(a), 4(b), 5(b), 5(e), 7(b), and 7(e)]. This is probably because the acceleration of the intrusion at the rapid growth in actual systems is more significant than that in the model. Moreover, the width of an intrusion within the pipe may also be related to the growth rate because it is smaller when $\mu_H \ll \mu_L$ than when $\mu_H \gg \mu_L$, as we have shown in our previous study (see Fig. 12 in [21]).

The present model also has a problem that the number of the parameters is large. Indeed, there are six parameters b_1, b_2, k, n, α, and γ to be specified experimentally. Moreover, their physical meanings are still unclear except α and γ. Thus, it is clearly needed to reduce the number of the parameters in the model through further investigation. Nevertheless, since these parameters have universal characters at least with regard to the viscosity and the pipe length, the present model is much more useful than the previously accepted model [11–13] which contains fully unknown parameters.

Although we have considered the effect of the viscosities of the fluids and the pipe length in the present study, other factors such as the densities of the fluids, pipe diameter, and interfacial tension between the fluid and pipe may also affect the behavior of a density oscillator. In addition, the present model is applicable in the limited case where $d \gg a$ and $\beta\sigma^{1/2} \ll 1$ are satisfied. Hence, further generalization of the model is clearly required in the future.

Finally, the importance of the present model should be noted in that it will provide a universal principle for relaxation oscillators that exhibit a repetitive change of slow and fast processes. In other words, it is considered that the three factors corresponding to F_1, F_2, and F_3 are essential for the onset of the fast process in a relaxation oscillator: the factor corresponding to F_3 "triggers" the change from the slow to the fast process and that corresponding to F_2 promotes the onset of the fast process when it overwhelms that corresponding to F_1. We expect that this finding will provide an essential breakthrough in the study of relaxation oscillations.

[1] M. V. L. Bennett and R. S. Zukin, Neuron **41**, 495 (2004).
[2] J. C. Dunlap, Cell **96**, 271 (1999).
[3] B. Blasius, R. Neif, F. Beck, and U. Lüttge, Proc. R. Soc. London, Ser. B **266**, 93 (1999).
[4] A. Kuznetsov, M. Kærn, and N. Kopell, SIAM J. Appl. Math. **65**, 392 (2004).
[5] R. J. Field and R. M. Noyes, J. Chem. Phys. **60**, 1877 (1974).
[6] K. Wiesenfeld, P. Colet, and S. H. Strogatz, Phys. Rev. E **57**, 1563 (1998).
[7] P. S. Landa, *Nonlinear Oscillations and Waves in Dynamical Systems* (Kluwer Academic, Dordrecht, 1996).
[8] A. Pikovsky, M. Rosenblum, and J. Kurths, *Synchronization: A Universal Concept in Nonlinear Sciences* (Cambridge University Press, Cambridge, 2001).
[9] Y. Kuramoto, *Chemical Oscillations, Waves, and Turbulence* (Springer-Verlag, Berlin, 1984).
[10] S. Martin, Geophys. Fluid Dyn. **1**, 143 (1970).
[11] K. Yoshikawa and H. Kawakami, Oyo Suri **4**, 238 (1994), in Japanese.
[12] K. Yoshikawa and K. Fukunaga, Chem. Phys. Lett. **174**, 203 (1990).
[13] K. Yoshikawa, S. Maeda, and H. Kawakami, Ferroelectrics **86**, 281 (1988).
[14] M. Okamura and K. Yoshikawa, Phys. Rev. E **61**, 2445 (2000).
[15] S. Nakata, T. Miyata, N. Ojima, and K. Yoshikawa, Physica D **115**, 313 (1998).
[16] K. Miyakawa and K. Yamada, Physica D **151**, 217 (2001).
[17] K. Miyakawa and K. Yamada, Physica D **127**, 177 (1999).
[18] K. Yoshikawa, N. Oyama, M. Shoji, and S. Nakata, Am. J. Phys. **59**, 137 (1991).
[19] O. Steinbock, A. Lange, and I. Rehberg, Phys. Rev. Lett. **81**, 798 (1998).
[20] M. Ueno, F. Uehara, Y. Narahara, and Y. Watanabe, Jpn. J. Appl. Phys., Part 1 **45**, 8928 (2006).
[21] T. Kano and S. Kinoshita, Phys. Rev. E **76**, 046208 (2007).
[22] T. Kano and S. Kinoshita, J. Korean Phys. Soc. **53**, 1273 (2008).
[23] H. Schlichting, *Boundary Layer Theory* (McGraw-Hill, New York, 1960).
[24] G. Taylor, Proc. R. Soc. London, Ser. A **201**, 192 (1950).